A user friendly statistical system for polarimetric SAR image classification

A. H. Correia*, c. da Costa Freitas*, A. c. Frery** and S. J. S. Sant' Anna*
**Instituto Nacional de Pesquisas Espaciais, Divisao de Processamento de lmagens, CP 525, 12201-970 Sao José dos Campos, SP - Brazil ({correia;corina;sidnei}@dpi.inpe.br)*
***Universidade Federal de Pemambuco, Departamento de Informática, CP 7851,50732-970 Recife, PE - Brazil (frery@di.ufpe.br)*

RESUMEN

En este artículo se presenta un sistema para la clasificación de imágenes SAR polarimétricas. Este sistema utiliza información contextual a través de un modelo Markoviano para las clases, además de modelos estadísticos para los datos. El sistema fue desarrollado pensando en el usuario y, por lo tanto, está íntegramente basado en interfaces gráficas. Toda vez que el usuario trata de activar una operación inválida, el sistema le informa la secuencia correcta de pasos. La funcionalidad del sistema se verifica clasificando áreas de cultivo, en una imagen SIR-C/X-SAR.

PALABRAS CLAVE: Clasificación, Contexto, Estadística, Radar de apertura sintética.

ABSTRACT

This article presents a system for polarimetric SAR image classification. This system uses contextual information through a Markovian model for the classes, besides a statistical model for the data. It is developed with the user in mind and, therefore, it is solely based on graphic user interfaces. The user is prompted with the correct sequence of steps whenever an invalid option is invoked. The functionality of the system is checked classifying a SIR-C/X-SAR image, where mainly crops are observed.

KEY WORDS: Classification, Context, Synthetic aperture radar, Statistics.

INTRODUCCION

The intensification of remote sensing studies in the field of Synthetic Aperture Radar (SAR) imaging sensors is leading towards a better understanding of the scattering mechanisms of terrestrial targets in the microwaves spectrum. Besides this, it has led to more dependable applications of SAR imagery and products to geology, cartography, and other fields of knowledge.

One of the most useful products of digital images is the result of automatic or semiautomatic data classification. This product is becoming more and more precise since the Gaussian hypothesis was weakened, and since better suited distributions for SAR data were incorporated into the process (Nezry et al., 1996; Frery et al., 1997a).

In Vieira (1996) this improvement becomes evident: it is shown that for monospectral SAR data, the simultaneous use of proper distribution for each class, along with contextual information, leads to better classifications than those obtained either by Gaussian fitting and/or by pointwise classification. On the other hand, the use of monospectral SAR data has its limitations.

The number of studies and applications involving polarimetric SAR data is increasing steadily. These data are formed by sending and receiving the electromagnetic signal in both horizontal and vertical polarisation and, thus, they mar carry a larger amount of information than that available from a single component. Though there is currently no sensor operating in different bands and polarisations, studies in this area are useful.

Several works are devoted to the statistical characterisation of single-look polarimetric SAR data. The reader is referred to DeGrandi et al. (1992), Kong, (1988), Lim et al. (1989), Quegan and Rhodes (1995), Yueh et al. (1989), to name a few.

The potential of multilook polarimetric data, where each value is the mean over several observations, is notorious as presented in Lee and GcuDes (1994) and in Lee et al. (1995), for instance. The statistical properties of this kind of data have not been fully exploited yet They have the advantage of exhibiting a speckle noise reduction as well as data reduction. The disadvantage is the resolution loss.

Given the potentiality of polarimetric data for image classification, there is a need for systems that use all the information of polarimetric data, in a manner that the user can handle it easily without knowing too much about the complexity of the underlying theory. The authors of this paper have no knowledge of such a system implemented in commercial software.

The objective this paper is to present a system for multilook polarimetric SAR image classification which was developed to assess the potential of this kind of data. The system is strongly based on the statistical properties of the data, and it uses a Maximum Likelihood (ML) classification as the initial configuration for a contextual Markovian classification technique: the Iterated Conditional Modes (ICM for short), presented in Vieira (1996). The system present in here allows the analysis of intensity, phase difference, ratio of intensities and intensity-phase data. These data formats are derived from multilook polarimetric SAR imagery, and their distributional properties are here recalled. The system is based on graphic user interfaces, and was developed as an extension of the ENVI (Environment for Visualizing Images) image processing system (ENVI, 1996).

POLARIMETRIC SAR SYSTEMS

Conventional SAR systems operate in a single frequency, with a single antenna of fixed polarisation for both the transmitted and received signals. Usually only the intensity or the amplitude data is supplied to the user and, as a consequence, any information carried in the phase of the complex electromagnetic signal is lost.

When polarimetric SAR sensors are used, the full complex signal is recorded and, thus, the return in all the configurations *(HH, H~ VH* and *VV)* are fully recorded (intensities or amplitudes and relative phases). In order to accomplish this for every resolution cell the complex scattering matrix, denoted as

$$S=\begin{pmatrix} S_{VV} & S_{VH} \\ S_{HV} & S_{HH} \end{pmatrix} \tag{1}$$

is measured. Subscripts *p, q* ∈ *{H, V}* denote the transmission and reception components of the signal, respectively, and elements S_{pq} are called *complex scattering amplitude.* Sarabandi (1992) shows that

$$S_{pq} = |S_{pq}|\, e^{i\phi_{pq}} = \sum_{n=1}^{N} |s_{pq}^{n}|\, e^{i\phi_{pq}^{n}} \tag{2}$$

where *N* is the number of scatterers of each resolution element, each having amplitude $|s_{pq}^{n}|$ and phase ϕ_{pq}^{n}.

Other ways of representing polarimetric data are the Stokes matrix, the modified Stokes matrix, the covariance matrix and the Mueller matrix (Ulaby and Elachi, 1990).

STATISTICAL PROPERTIES OF POLARIMETRIC SAR DATA

Data obtained with coherent illumination, as is the case of SAR data, are corrupted by a signal-dependent noise called *speckle.* A usual model for the signal and this noise is the Multiplicative Model. It states that, under certain conditions (Tur et al., 1982) the observed value in every pixel is the outcome of the random variable $Z = XY$, where X is the random variable that models the *backscatter* and *Y* is the one that models the speckle noise, and fuese last two variables are independent.

Statistical models for multilook polarimetric data are derived from the covariance matrix, which exhibit a complex Wishart distribution (Lee and Grunes, 1992; Du and Lee, 1996).

Ullaby and Elachi (1990) show that, for satellites that transmit and receive through the same antenna (which is the usual case), it is possible to suppose that $S_{HV} = S_{YH}$ Therefore, the matrix presented in equation (1) can be reduced, without loss of information to

$$Z=\begin{pmatrix} S_1 \\ S_2 \\ S_3 \end{pmatrix} \tag{3}$$

where S_i , $1 \le i \le 3$ denotes S_{HH} , S_{HV} and S_{VV} in any convenient order.

When the number of elementary scatterers (denoted *N* in equation (2)) is very large, it can be assumed that the vector Z in equation (3) obeys a multivariate complex Gaussian distribution (Goodman, 1963). This is true if the backscatter X is constant, independently of the imaged area, since the speckle Y is assumed to obey a mu1tivariate complex Gaussian law.

In this work mu1tilook data are considered and, in order to derive their distributional properties, vector Z in equation (3) will be, thus, considered the *k-th* single-look observation and denoted as *Z(k).* A fixed number, *n,* of independent outcomes of Z are averaged to form the *n-1ooks* covariance matrix, given by (Lee et al., 1995)

$$Z^{(n)} = \frac{1}{n}\sum_{k=1}^{n} Z(k)\, Z^{*}(k)^{T} \tag{4}$$

where $Z^{*}(k)^{T}$ denotes the transposed conjugate of *Z(k).*

The advantage of working with the covariance matrix, defined as $A = nZ^{(n)}$, is that it exhibits a multivariate complex Wishart distribution (Srivastava, 1963). Its density is given by

$$p_{Z^{(n)}}(z)=\frac{n^{qn}\,|z|^{(n-q)}\,\exp[-nTr(C^{-1}z)]}{K(n,q)|C|^{n}} \qquad (5)$$

where *q* denotes the dimension of the vector Z, $K(n,q) = \pi^{q(q-1)/2}\,\Gamma(n)...\Gamma(n-q+1)$, Tr denotes the trace of the matrix, $C = E[ZZ^{*T}]$, and Γ is the Eu1er Garnma function. Using equation (5) it is possible to derive the densities for situations of particular interest, as presented in Lee et al. (1995). They are addressed here for a better understanding of the implemented classifiers. The following situations were implemented in the system here considered: a pair of intensities, phase difference, ratio of intensities and pair intensity-phase.

CONTEXT, THE POTTS-STRAUSS MODEL AND THE ICM ALGORITHM

The use of Markovian distributions (also known as Markov random fie1ds) for the parametric modelling of context dates back to the 70s, but their use became widespread after the work by Geman and Geman (1984).

Markov random fields, are a mu1tidimensional extension of the index of Markov chains, where the concept of *future* given *past* is transformed into spatial conditioning. The interest in this kind of distributions dates back to the beginning of the century, since the well-know Ising model for magnetism is one of its most famous particular cases. The reader is referred to (Besag, 1989) for more information about their use in image analysis. For the purpose of this paper, it will suffice to define the underlying distribution for the classes: the Potts-Strauss modelo

Denote $\bar{\eta}=[\eta_s, s \in S]$ a particular configuration of classes, with S the set of co-ordinates of the image. Any $\bar{\eta}$ will be regarded as the outcome of the random variable defined as $W: \Omega \rightarrow \Xi^s$, where Ω. is a sample space and $\Xi=\{\xi_1 - \xi_2\}$ is the set of all possible classes for each co-ordinate, and Ξ^s is the set of all possible maps (completely classified images).

Markov random fields are specifications of probabilities to every map $\bar{\eta}=\Xi^S$, satisfying some mild conditions. These probabilities can be chosen in arder to model spatial interaction. This modelling would be attained by associating higher (lower, resp.) probability values to more (less, resp.) ordered -smooth, less varyingmaps. For the definition of the techniques embedded in the system here considered, fuese probabilities depend on $\bar{\eta}$ and on a single real parameter β.

If the random variable M (for "map") obeys the distribution given by

$$\Pr(M=\tilde{\eta}) = Z_{\beta}^{-1}\exp\left(\beta\sum_{(s,t)} 1_{\eta_t}(\eta_s)\right) \qquad (6)$$

where Z_β is a normalising constant, 1_A is the indicatar function of the set *A,* and *(s,t)* denotes that co-ordinates s and t are neighbours, then it is said that M obeys the Potts-Strauss model with parameter β. It is important to notice that for every β> 0 this model favours those configurations that exhibit clusters of same-class pixels.

Once defined this distribution, it can be used as the prior for the classes in a Bayesian framework. Every class $\xi_l \in \Xi$, $1 \le i \le l$, will be associated to a certain type of target.

For a discussion of the possible ways to obtain estimators of $\bar{\eta}$ (the true map) given the data, the reader is referred to Besag (1989). The system here presented implements one of fuese estimation techDiques: the Iterated Conditional Modes (ICM).

Assuming that the classes can be described by the Potts-Strauss model, the problem of classification consists of finding an estimator of the *true* class configuration $\bar{\eta}$ given the data. It will also be assumed that the distribution of the data given the classes is known, after the training steps required by the ML procedure.

The ICM algorithm consists of the iterative improvement of the classification of the co-ordinates, using the information of its return and the classes of its neighbouring sites. Denoting $\bar{\eta}(k)$ the available classification after the *k-th* iteration, this classification will be improved replacing the class observed in every site s by the class $\xi' \in \Xi$ that maximises theexpression

$$L(\xi') = f_{\xi'}(z_s)\exp\left(\beta\#\{t\in\partial_s : \xi_t = \xi'\}\right) \qquad (7)$$

where f_ξ ,is the density associated to class ξ'and δ_s is the set of neighbouring co-ordinates around site s. The relevant densities for the problem at hand are presented in the next section. The process iterates until there is evidence of convergence.

Equation (7) is the conditional likelihood of class ξ' given the data and the neighbouring classes. The first term alone would have yielded to the ML classification scheme, while the second alone leads to the mode filter (the replacement of the current class by the most frequently observed one in its neighbourhood).

EQUIVALENT NUMBER OF LOOKS ESTIMATION

The equivalent number of looks *n* is one of the parameters of the distributions arising from the multiplicative modelo This parameter could be estimated only once for the whole image, using samples selected ayer homogeneous region. This means, for linear detection (amplitude data) that fuese should be samples from $\Gamma^{1/2}$ distributions (Frery et al., 1997a).

The interactive procedure implemented to estimate the equivalent number of looks here described was proposed in Vieira (1996).

Several samples may be selected, and χ^2 goodness-of-fit test for the $\Gamma^{1/2}$ distribution is performed for each sample. The sample with low likelihood of belonging to the $\Gamma^{1/2}$ distribution (low p-values) may be discarded, and the final estímate is computed as the mean of the remaining estimated values. The user has the option of the decorrelating the samples (i.e. of resampling in lines and columns) by defining the horizontal and vertical lags. To help the user in this task, the system calculates the autocorrelation function of the data. The interface s for the calculating the autocorrelation function of samples for the χ^2 test, and the estimation of *n,* are shown in Figure 1, Figure 2 and Figure 3, respectively.

THE SYSTEM

The system behaves as an extension of fue ENVI v. 2.5 system, and it uses its native functions and others from IDL *(lnteractive Data Language).* In this inanner, several functions such as those for data management, processing and analysis were reused.

Both classifications implemented are supervised and, thus, require the specification of training sets for parameter estimation. These sets are informed through *regions of interest,* previously defined by the used with ENVI utilities. The equivalent number of looks *(n* in equations (4) and (5)) is also an input parameter; it can be estimated within the system presented in Vieira (1996) and described in the previous section.

The ICM classification method is a contextual procedure that, in order to classify every pixel, uses both the observed value in the corresponding coordinate and the classification of the surrounding sites. In order to incorporate this context within a statistical framework, the Potts-Strauss is used for the classes.

The system here presented uses an inference technique called *pseudolikelihood,* in order to estimate the required parameter of the Markovian model (β in equation (6)). This technique alleviates the user from the need of choosing parameters in a trial-and-error basis, a major drawback of most advanced classification algorithms. Details are available in Vieira (1996), Vieira et al. (1997) and in Frery et al. (1997b). The current implementation uses any existing classification as starting point, being the ML the default.

The following subsections describe the functionality of the system, in every case for *n* looks intensity data. The densities and parameter estimators are as presented in Lee et al. (1995).

ICM intensity bivariate

This option applies the ML and ICM classifications to a pair of intensity images, either two polarimetric components or the result of two passages of the same monospectral sensor (such as JERS-l, ERS-l, etc.).

After the input of the initial data the interface shown in Figure 4 is presented. It exhibits the 2-D histogram of the pair of bands, along with the 2-D estimated density, both in perspective and in contour plot. The estimated parameters are presented at the bottom of the plots.

As every interface presented in this work, that presented in Figure 4 is fully interactive with the user The user can specify the interval the plots will be drawn, any desirable rotation, the number of contour levels to be used, etc. This feature greatly stimulates the interaction of the user with the data. The input values affect all the sub-windows, since they are connected in order to help the visualisation.

This interface has to be used for every class of interest. Once this is performed, the ML classification is performed, and the interface shown in Figure 5 is presented to the user. The user can interactively choose the classes for which the estimated densities are presented (in perspective and as a contour plot). The user can specify the viewpoint and number of (evenly spaced) contour levels. Each class is associated to an unique colour.

The ML classification is produced, and used as initial configuration by the ICM algorithm. This iterative technique stops according to the number of co-ordinates whose classification changes from one iteration to the next (Vieira, 1996).

Denoting as R_1, R_2 the pair of intensities, their joint density under the model characterised by equation (5) is

$$p(R_1,R_2)=\frac{n^{n+1}(R_1R_2)^{\frac{(n-1)}{2}}\exp\left(-\frac{n\left(\frac{R_1}{H_{11}}+\frac{R_2}{H_{22}}\right)}{1-|\rho_c|^2}\right)}{(H_{11}H_{22})^{\frac{(n+1)}{2}}\Gamma(n)(1-|\rho_c|^2)|\rho_c|^{n-1}}I_{n-1}\left(\frac{2n|\rho_c|}{1-|\rho_c|^2}\sqrt{\frac{R_1R_2}{H_{11}H_{22}}}\right)$$

where $H_{11} = E[R_1]$ and $H_{22} = E[R_2]$, I_{n-1} denotes the modified Bessel function of order n-1, and

$$\rho_c=\frac{E[S_iS_j^*]}{\sqrt{E[|S_i|^2]E[|S_j|^2]}}=|\rho_c|e^{i\theta}$$

The parameter $|\rho_c|$ can be estimated by selecting a sample of size *m* and computing

$$\hat{\rho}=\frac{\sum_{i=1}^{m}[(R_{1i}-\overline{R}_1)(R_{2i}-\overline{R}_2)]}{\sqrt{\sum_{i=1}^{m}[(R_{1i}-\overline{R}_1)^2]\sum_{i=1}^{m}[(R_{2i}-\overline{R}_2)^2]}}$$

Where $\bar{R}_1$ and $\bar{R}_2$ denote the sample means of R_1 and R_2, respectively.

ICM phase difference

This option applies the ML and ICM classifications to Ψ, the difference between the phases of two complex images. These images are derived from two components $S_i(k)$ and $S_j(k)$ of single-look images (equation (3)) in the following manner:

$$\psi = \arg\Big|\overbrace{\frac{1}{n}\sum_{k=1}^{m} S_i(k)S_{j_1}^*(k)}^{R_{ij}^{(n)}}\Big| = \tan^{-1}\left[\frac{\Im[R_{ij}^{(n)}]}{\Re[R_{ij}^{(n)}]}\right]$$

where ℜ and ℑ denote, respectively, real and imaginary parts.

After the required parameters have been introduced, the interface shown in Figure 6 is presented, with the histogram of the data, the fitted density and estimated phase difference parameters. When every class has been checked with this interface, Figure 7 is shown. This interface presents the estimated densities of the phase difference for every considered class, allowing the visual assessment of their separability throughout this feature.

The density of the quantity defined above, under the aforementioned model, is given by

$$p_{\psi}^{(n)}(\psi) = \frac{\Gamma(n+1/2)(1-|\rho_c|^2)^n\beta}{2\sqrt{\pi}\,\Gamma(n)(1-\beta^2)^{n+1/2}} + \frac{(1-|\rho_c|^2)^n}{2\pi}F(n,1;1/2;\beta^2)$$

where $-\pi < \psi \le \pi$, $b=|\rho_c|\cos(\psi-\theta)$, θ is the phase of the complex coefficient of correlation and $F(n,1;1/2;\beta^2)=2F_1(n,1;1/2;\beta^2)$ is the Gaussian hypergeometric function. In the system this function was implemented based on the algorithm described in Press et al. (1988), for any $n > 0$.

ICM ratio of intensities

Both the ML and ICM classification are obtained, derived from the ratio between two multilook in tensity bands, i.e., using data of the form R_i/R_j.

Analogously to the previous situation, namely for the classification using phase difference, after the required inputs the histogram, fitted densities and estimated parameters are shown for every class. Once the fittings have been checked for every class, the whole set of fitted densities is shown.

The density that characterises this data is

$$p^{(n)}(w) = \frac{\tau^*\Gamma(2n)(1-|\rho_c|^2)^n(\tau+w)w^{n-1}}{\Gamma(n)\Gamma(n)[(\tau+w)^2-4\tau|\rho_c|^2 w]^{(2n+1)/2}}$$

where $w = R_1/R_2$ and $\tau = H_{11}/H_{22}$

Though, from the theoretical point of view the denominator in R_1/R_2 will take positive values with probability 1, the fact of dealing with discrete data imposes the use of a "safe" ratio. The system works with $R_1/\max\{R_2,1\}$, which eliminates the possibilit y of an overflow.

Intensity and phase ICM SAR

This option calculates both the ML and ICM classification, using a multilook intensity image R_1 and a phase difference ψ. The input data for this processing are two multilook bands Ri and R_j, and the corresponding multilook complex image $R_{ij}^{(n)}$ (see equation (8)).

The rest of the process is as presented in previous sections, namely the same as for classification using a pair of intensities.

In order to derive the joint density of R_1 and ψ, intensity and phase difference data obtained from two components S_i and S_j of the scattering matrix, consider the image

$$p^{(n)}(w) = \frac{\tau^*\Gamma(2n)(1-|\rho_c|^2)^n(\tau+w)w^{n-1}}{\Gamma(n)\Gamma(n)[(\tau+w)^2-4\tau|\rho_c|^2 w]^{(2n+1)/2}}$$

The joint density of B_1 and ψ is given by

$$p(B_1,\psi) = \frac{B_1^{n-1}\exp\left(-\frac{B_1}{1-|\rho_c|^2}\right)}{2\pi\,\Gamma(n)}\,{}_1F_1\left[1;\frac{1}{2};\frac{\beta^2}{1-|\rho_c|^2}B_1\right] + \frac{\beta B_1^{n-\frac{1}{2}}\exp\left(-\frac{B_1(1-\beta^2)}{1-|\rho_c|^2}\right)}{2\pi\,\Gamma(n)\sqrt{1-|\rho_c|^2}}$$

where $w = R_1/R_2$ and $\tau = H_{11}/H_{22}$

Though, from the theoretical point of view the denominator in R_1/R_2 will take positive values with probability 1, the fact of dealing with discrete data imposes the use of a "safe" ratio. The system works with $R_1/\max\{R_2,1\}$, which eliminates the possibilit y of an overflow.

Intensity and phase ICM SAR

This option calculates both the ML and ICM classification, using a multilook intensity image R_1 and a phase difference ψ. The input data for this processing are two multilook bands Ri and R_j, and the corresponding multilook complex image $R_{ij}^{(n)}$ (see equation (8)).

The rest of the process is as presented in previous sections, namely the same as for classification using a pair of intensities.

In order to derive the joint density of R_1 and ψ, intensity and phase difference data obtained from two components S_i and S_j of the scattering matrix, consider the image

where ${}_1F_1$ is the confluent hypergeometric function.

In the system this function was implemented by means of an adaptation of the Gaussian hypergeometric function algorithm described in the Press et al. (1988).

CASE STUDY

In order to assess the information content of polarimetric SAR data in crops areas, a *SIR-C/X-SAR* image was analysed.

As presented in the previous section, the system offers a wide variety of options for input data. All these possibilities were tested, namely bivariate intensity, phase difference, ratio of intensities and the pair intensity-phase. For each of fuese tour options the ML classification was obtained and used as initial configuration for the ICM algorithm.

Data and preliminary analysis

The main parameters of the space shuttle image under study are presented in Table 1. The central co-ordinates of the area are 09(07' S, 40(18' W. The imaged area corresponds to an irrigated region where several types of crops are observed.

Figure 8 presents two compositions of the data set under study. To the left (right, resp.) the red, green and blue channels were associated to the L (C resp.) band and polarisations HH, HV and VV. This images also present the test (right) and training (left) sets.

The classes analysed in this work are presented in Table 2, where their respective colour keys (the colours with which they will be represented in the classifications), number of training and test samples and sizes of these samples are also shown. These classes are river (that will be depicted in blue), a steppe vegetation type called *caatinga* (green), prepared soil (red), soy (magenta), tillage (cyan) and corn (yellow).

Though, as presented in Table 1, the nominal number of looks is 4.7854018, the estimated quantity amounts to 2.97479. This value is the mean of the equivalent number of looks observed in each component (see Table 3). The estimation of this quantity was performed using samples as large as possible, and taken over homogeneous areas. Before using these samples, they were submitted to χ^2 goodness of fit test, and they all passed at the 1 % level of significance the hypothesis of being homogeneous areas.

Comparison of classifications

All possible combinations of data for same band were used to generate classifications, as described in Correia (1998). These precision of these results was assessed with the use of the estimated Kappa ($\hat{k}$) coefficient of agreement and its sample variance (s_k^2) over test areas (Landis and Koch, 1977).

The quantitative comparison of results, when bivariate intensity data are used, is presented in Table 4. The best classification achieved (namely for the L HVVV data set) is highlighted. Similar results, obtained with phase difference, with the ratio of intensities and with the pair intensity-phase are presented in Table 5, Table 6 and Table 7, respectively. In all these tables the best results are highlighted.

The analysis of these tables shows that classifications obtained with phase difference C HH-HV data leads to the worst overall results, for both ML and ICM methods. These two classifications are shown in Figure 9.

It is also noticeable that phase difference data from HH-HV and HVVV polarisations, from both L and C bands, do not carry useful information about the studied areas and can, therefore, be discarded from the Test of the comparisons. Classifications using these data sets were assessed in Table 5, since the system allows it.

Taking into account the results obtained with the other data sets for L band, it can be concluded that

1. The worst ML classification was obtained with the ratio of HHVV intensities, and the best with the HVVV pair of intensity data (see Figure 10). The improvement from the worst to the best ML classification is, in this case, of 475,77%.
2. The worst ICM classification was obtained when using ratio of HH-HV intensities, and the best was attained when the initial configuration was the best ML classification, i.e., when the HV-VV pair of intensity data was used (Figure 11). The improvement, in this case, is of314,74%.

Discarding the HH-HV and HVVV phase difference data sets, and considering C band data, it can be concluded that

1. The worst ML classification was obtained with the ratio of HHVV intensities, and the best with the HV-HV pair of intensity data. The obtained improvement from the worst to the best ML classification is of 523,22%.
2. The worst ICM classification was obtained when using ratio of HHVV intensities, and the best was attained when the initial configuration was the best ML classification, i.e., when the HH-HV pair of intensity data was used (Figure 12). The improvement, in this case, is of 365,42%.

Comparing the best ML and ICM results, for each band, it can be concluded that ICM improves 28,14% ML the classification in L band, and 20,38% in C band. It is interesting to compare ML and ICM results, since the latter is an improved result that used the former as starting point. The improvement is notorious, both from the qualitative point of view (regions are smoother and better defined) and from the quantitative one.

Though the aforementioned improvement is welcome in every application, it is not as dramatic

as that obtained in Frery et al. (1997b) and Vieira (1996). In that work improvements of the order of 500% were obtained when comparing ML and ICM classifications. This might be due to, among other reasons, the fact that in those works a single component amplitude multilook data were used, which conveys les s information per pixel than that carried by polarimetric images.

The analysis of the confusion matrices (not shown here, but available. through the system) shows that, using the ICM algorithm in all cases, the best results are

l. For the class River, the pair intensity HH-HV band C yielded to a 100% of correctly classified pixels (Figure 12, right).
2. The class *Caatinga* was best classified (98% of correctly labelled pixels) with the pair intensity HVVV band C (Figure 13, left).
3. Phase difference between HHVV band C data yielded to the best Soil classification (94%, Figure 12 left).
4. The Soy class was best classified through the use of intensity HH-VV pair, from L band (Figure 13, right).
5. The pair phase-intensity, from HHVV L band, yielded to the best Tillage classification (95%, Figure 14).
6. The best (86%) Corn classification was obtained when the intensity par HV-VV data set from L band was used (Figure 10, right).

These results show that the overall performance criterion, namely the estimated Kappa ($\hat{k}$) coefficient of agreement, mar not inform how well individual classes are classified. Besides this, these results show the importance full polarimetric images, since the information they convey is rather specialised and in concentrated in different data sets for different classes.

CONCLUSIONS AND FUTURE WORK

The system here presented allowed the comparison of classifications using four types of multilook polarimetric data: bivariate intensity, phase difference, ratio of intensities and the pair intensity-phase.

This system is user friendly and goal driven, and it proved being easy to use. The users is only required to know the basic ideas of maximum likelihood classification, in order to be able to produce improved results based on the Markovian modelling of classes and pseudolikehood estimation.

The intense use of graphic interfaces eases the modelling and understanding of data, a central issue in SAR image analysis.

A SIR-C/X-SAR image of mainly crops was chosen as case study. Training and test samples were chosen and analysed within the system, and all possible data configurations for each band were classified. The best (worst) ICM overall classification was obtained with the band L, HVVV intensity pair (band C, HH-HV phase difference, resp.) data.

Using the ICM algorithm yields to classifications not worse than the initial one. Since in this study all initial classifications were obtained by the ML method, improvements from this pointwise classification technique were expected. In fact, as presented, significant improvements were achieved at the mere expense of CPU time.

The version of the system here presented only allows the use of distributions associated to homogeneous regions. The authors are currently upgrading the functionality of the procedures, in order to allow the use of other distributions, more suited to heterogeneous and extremely heterogeneous observations.

ACKNOWLEDGEMENTS

This work was partially developed with resources from CNPq (Proc. 523469/96-9) and FACEPE (APQ 0707-1.03/97).

BIBLIOGRAPHY

BESAG, J. 1989. Towards Bayesian image analysis. J. App. Stat. 16(3):395-407.

CORREIA, A.H. 1998. Desenvolvimento de classificadores de máxima verossimilhanr;a e ICM para imagens SAR polarimétricas. (MSc in Remote Sensing) Insti tuto de Nacional de Pesquisas Espaciais. Sao José dos Campos, SP, Brazil. To be presented.

DEGRANDI, G.; LEMOINE, G. and SIEBER, A. 1992. Supervised fully polarimetric classification: an experimental study on the MAESTRO-1 Freiburg data seto In: IGARSS'92 International Geoscience and Remote Sensing Symposium'92, Houston. Intemational Space Year: space remate sensing. IEEE, V. 1, p. 782-785.

DU, L.J. and LEE, J.S. 1996. Polarimetric SAR image classification based on target decomposition theorem and complex Wishart distribution. In: IGARSS'96 International Geoscience and Remote Sensing Symposium'96, Lincoln. Remote Sensing for a Sustainable Future. IEEE, v. 1, p. 439-441.

ENVI 2.5 user's guide: The Enviromment for Visualizing Images, version 2.5. 1996. Lafayette, Better Solutions Consulting, 1993-1996. Under contract of Research Systems Inc.

FRERY, A.C.; MÜLLER, H.J.; YANASSE, C.C.F and SANT' ANNA, S.J.S. 1997a. A model for extremely heterogeneous clutter. IEEE Trans. Geosc. Rem. Sens. 35(3):648-659.

FRERY, A.C.; YANASSE, C.C.F.; VIEIRA, P.R. SANT' ANNA, S.J.S. and RENNÓ, C.D. 1997b. A user-friendly system for synthetic aperture radar image classification based on grayscale distributional properties and contexto Simp6sio Brasileiro de Computa~ao Gráfica e Processamento de Imagens, 10., 1997, p. 211-218. SIBGRAPI97. Los Alámitos, CA, IEEE Computer Society.

GEMAN, D. and GEMAN, S. 1984. Stochastic relaxation, Gibbs distributions and the Bayesian restoration

of images.IEEETrans. Patt. An. Mach.Int. 6(6): 721-741.

GOODMAN, N. R. 1963. Statistical analysis based on a certain multivariate complex Gaussian distribution. Ann. Math. Stat. 34(1):152-177.

KONG, J.A. 1988. Identification of terrain cover using the optimal polarimetric classifier. J. Electrom. Waves Appl.2(2):171-194.

LANDIS, J. and KOCH, G.G. 1977. The measurements of observer agreement for categorical data. Biometrics. 33(3):159-174.

LEE, J. S. and GRUNES, M. R. 1992. Feature classifica tion using multi-look polarimetric SAR imagery. In: IGARSS'92 Intemational Geoscience and Remote Sensing Symposium'92, Houston.Intemational Space Year: space remate sensing.IEEE, v. 1, p. 77-79.

LEE, J.S.; HOPPEL, K.W. and MANGO, S.A. 1994. Intensity and phase statistics of multi-look polarimetric and interferometric SAR imagery. IEEE Trans. Geosc. Rem. Sens. 32(5):1017-1028.

LEE, J.S.; DU, L.; SCHULER, D.L. and GRUNES, M.R. 1995. Statistical analysis and segmentation of multilook SAR imagery using partial polarimetric data. In: IGARSS'95 Intemational Geoscience and Remote Sensing Symposium'95, Firenze. Quantitative Remote Sensing for Science and Applications. Piscataway, IEEE, v. ni, p. 1422-1424.

LEE, J.S. and GRUNES, M.R. 1994. Classification of multilook polarimetric SAR imagery based on complex Wishart distribution. Int. J. Rem. Sens. 15(11): 2299-2311.

LIM, H.H; SWARTZ, A.A.; YUEH, H.A.; KONG, J.A.; SHIN, R.T. and VAN ZYL, J.J. 1989. Classifications of earth terrain using polarimetric SAR images. J. Geophys. Res. 94(B6):70497057.

NEZRY, E.; LOPÉS, A.; DUCROT-GAMBART, D.; NEZRY, C. and LEE, J.S. 1996. Supervised classification of K -distributed SAR images of natural targets and probability of error estimation. IEEE Trans. Geosc. Rem. Sens. 34(5):1233-1242.

PRESS, W.H.; FLANNERY, B.P.; TEULOSKY, S.A. and VE1TERLING, W.T. 1988. Numerical recipes in C, Cambridge, Cambridge University Press.

QUEGAN, S. and RHODES, l. 1995. Statistical models for polarimetric data: consequences, testing and validity.Int. J. Rem. Sens. 16(7):1183-1210.

SARABANDI, K. 1992. Derivations of phase statistics from the Mueller matrix. Radio Sci. 27(5):553-560.

SRIVASTAVA, M.S. 1963. On the complex Wishart distribution. Ann. Math. Stat. 36(1):313-315.

TUR, M.; CRIN, K.C. and GOODMAN, J.W. 1982. When is speckIe noise multiplicative? Appl. Opto 21:1157-1159.

ULABY, F. T. and ELACHI, C. 1990. Radar polarimetriy for geoscience applications. Norwood, Artech House, 364p.

VIEIRA, P.R. 1996. Desenvolvimento de classl:ficadores de máxima verossimilhanr;a e ¡CM para imagens SAR. (MSc in Remote Sensing) Instituto de Nacional de Pesquisas Espaciais. Sao José dos Campos, SP, Brazi1, 251 p. (INPE-6124-TDI/585).

VIEIRA, P.R.; YANASSE, C.C.F.; FRERY, A.C. and SANT' ANNA, S.J.S. 1996. Um sistema de aná1ise e classificasao estatísticas para imágens SAR. In: Primeras Jornadas Latinoamericanas de Percepción Remota por Radar, Buenos Aires, Dez. 1996. Técnicas de Processamiento de Imágenes. Paris, ESA, p. 170-185.

YUEH, S.H.; KONG, J.A.; JAO, J.K.; SHIN, R.T. and NOVAK, L.M. 1989. K-distributition and polarimetric terrain radar clustter. J. Electrom. Waves Appl. 3(8): 747-768.

Image identifier	P-11534
Acquisition date	April 14th 1994
Size o fue considered image	407 x 370 pixels
Frequency	L (1.254 GHz) and C(5.304G Hz)
Polarisation	HH,HV, WandVH
Incidence angle	49.496°
Platform height	216.14 km
Orbit direction	Descending
Type of product	Multilook Complex (MLC)
Nominal number of looks	4.7854018
Geometric representation	Ground range
Pixel spacing	12.5m in e and 12.5m in azimuth

Table 1. SIR-C/X-SAR image main parameters

Classes	Colour	Training samples		Test samples	
		Number	Pixels	Number	Pixels
River	Blue	2	4949	2	3844
Caatinga	Green	5	5177	5	3585
Prepared soil	Red	1	3221	1	2101
Soy	Magenta	2	2609	2	2128
Tillage	Cyan	1	635	1	360
Corn	Yellow	2	3505	2	1946

Table 2. Classes of interest, colour keys. training and test samples

	Band	
Polarisation	**L**	**C**
HH	2.6688	2.6713
HV	3.1836	2.9723
W	3.5340	2.8188
Mean	**2.97479**	

Table 3. Estimated equivalent numbert of looks in all the available bands and polarisations, and overall mean

Input data (band - polarisation)	$\hat{k}$		Variance (x 10^{-3})	
	ML	ICM	ML	ICM
L HH-HV	0.596980	0.710471	2.38412	1.99384
L HH-VV	0.575008	0.694241	2.48444	2.14506
L HV-VV	0.606424	0.777114	2.35719	1.64955
C HH-HV	0.575344	0.692635	2.50954	2.10982
C HH-VV	0.482214	0.571004	2.61262	2.72449
C HV-VV	0.566975	0.614171	2.68826	2.90562

Table 4. Assessment of classification precision using bivariate intensity data

Input data (band - polarisation)	$\hat{k}$		Variance (x 10^{-3})	
	ML	ICM	ML	ICM
L HH-HV	0.020904	0.025786	2.56678	3.39736
L HH-VV	0.193186	0.372729	2.68909	3.12572
L HV-VV	0.008927	0.014442	2.66556	5.07250
C HH-HV	-0.001943	-0.008580	2.06280	2.23533
C HH-VV	0.092317	0.148819	3.19603	4.39456
C HV-VV	0.005144	0.007090	2.62186	3.37758

Table 5. Assessment of classification precision using phase difference data

Input data (band - polarisation)	$\hat{k}$		Variance (x 10^{-3})	
	ML	ICM	ML	ICM
L HH-HV	0.105324	0.187371	3.12436	3.90025
L HH-VV	0.272400	0.360187	2.74605	3.37850
L HV-VV	0.318741	0.455631	2.57741	2.70515
C HH-HV	0.116141	0.165443	3.19497	4.82030
C HH-VV	0.181810	0.274525	3.71316	4.92802
C HV-VV	0.203089	0.272691	2.76586	3.36486

Table 6. Assessment of classification precision using the ratio of intensities data

Input data (band - polarisation)	$\hat{k}$		Variance (x 10^{-3})	
	ML	ICM	ML	ICM
L HH-HV	0.469581	0.633668	2.63720	2.34108
L HH-VV	0.325979	0.424540	2.77930	2.85456
C HH-HV	0.418908	0.521662	2.59719	2.55940
C HH-VV	0.416235	0.565799	2.65869	2.74780

Table 7. Assessment of classification precision using the the pair intensity-phase data

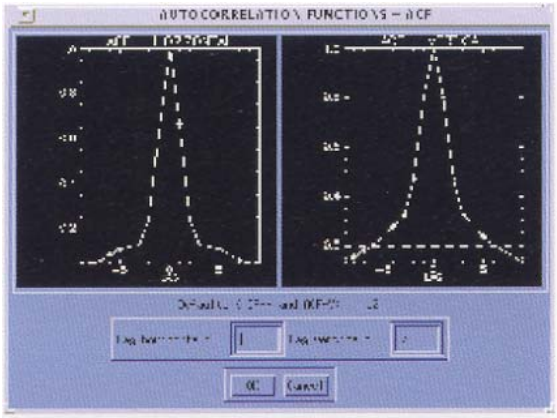

Figure 1. Etimated autocorrelation function in horizontal and vertical lags, for the estimation of the equivalent number of looks

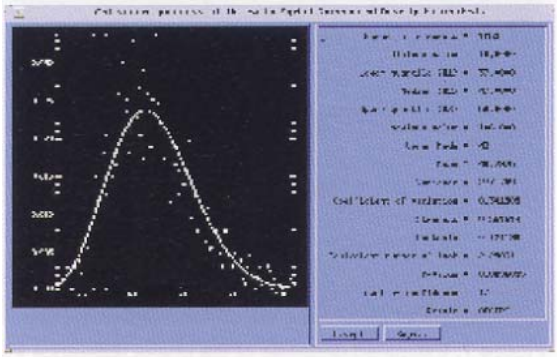

Figure 2. Interface of the χ^2 goodness of fit test for the estimatión of equivalent number of looks

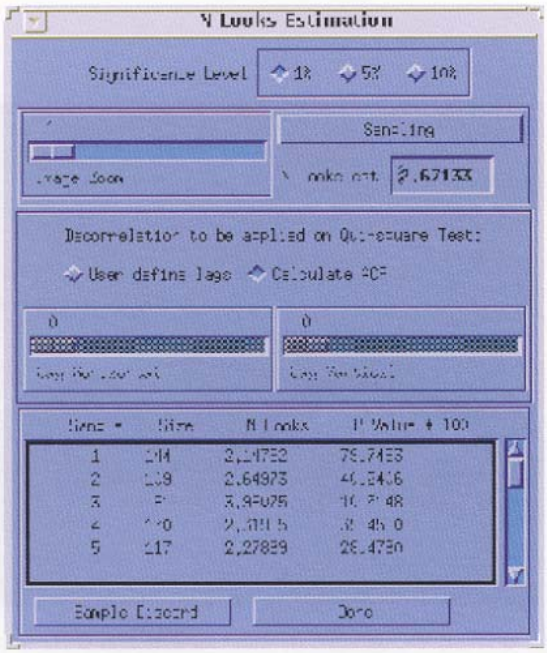

Figure 3. Interface for the estimation of the equivalent number of looks, with interactive choice of suited samples

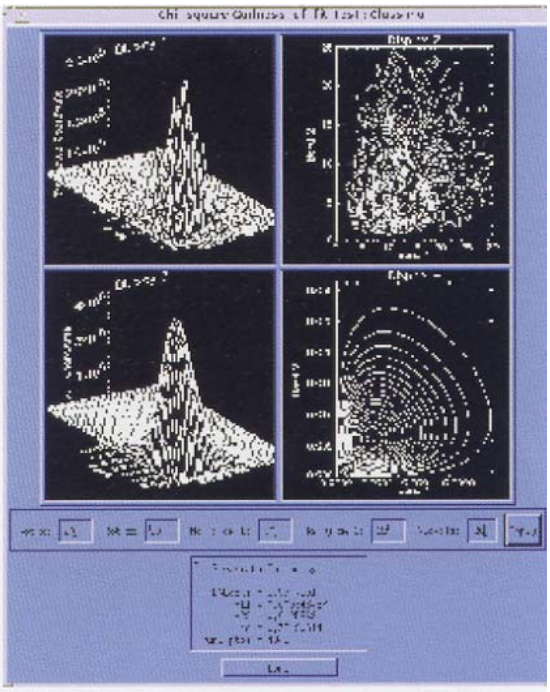

Figure 4. Density, 2-D histogram, contour plot and estimated parameters of two multilook intensity bands

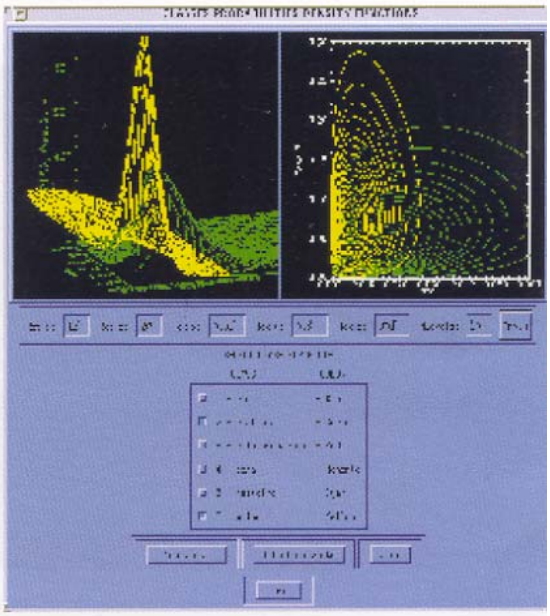

Figure 5. Densities associated to different classes of interest

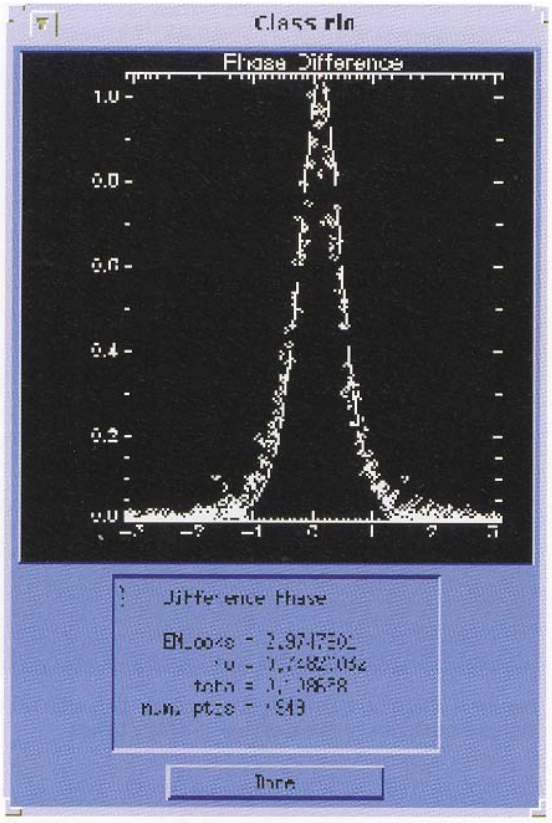

Figure 6. Histogram, fitted density and estimated phase difference parameters

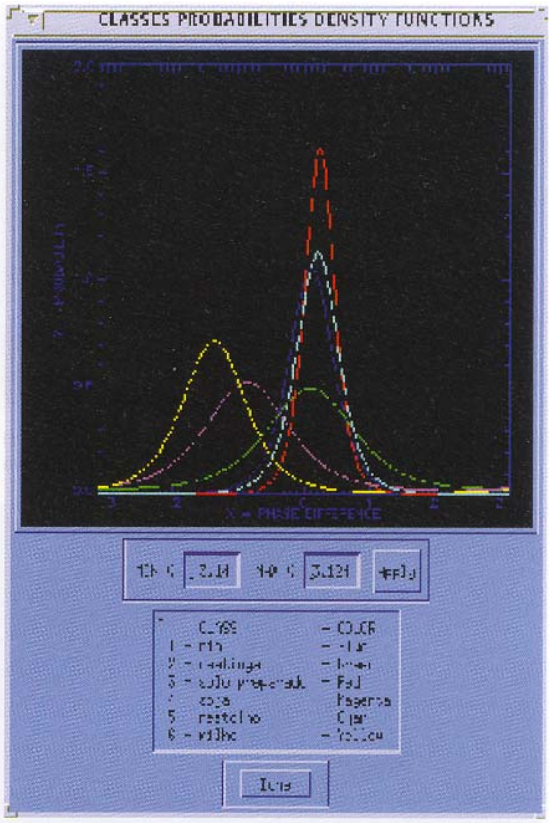

Figure 7. Estimated densities of the phase difference for every considered class

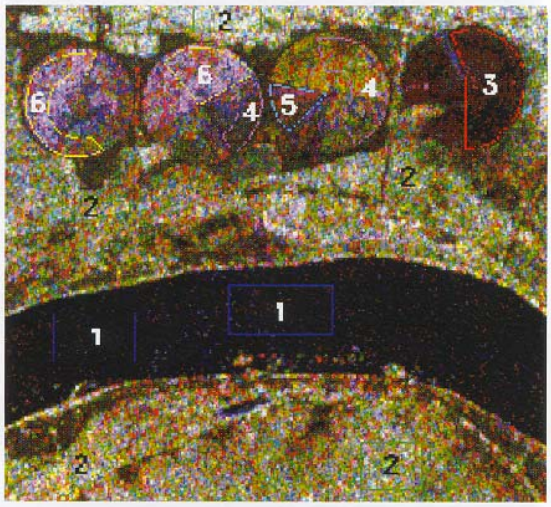

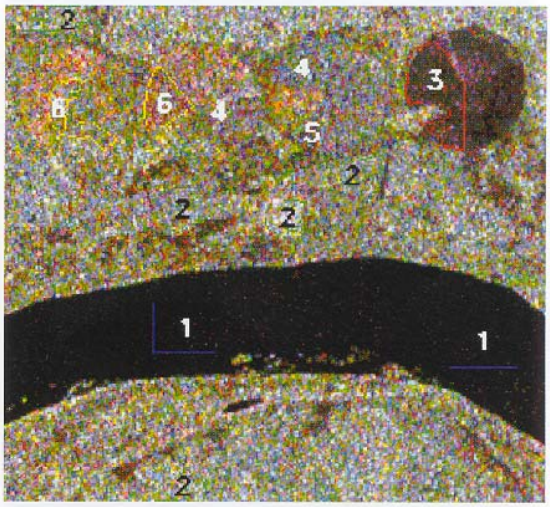

Figura 8. Two colour compositions of the original data R-HH, G-HV, B-VV, bands L (r) with test sets and C (1) with training sets

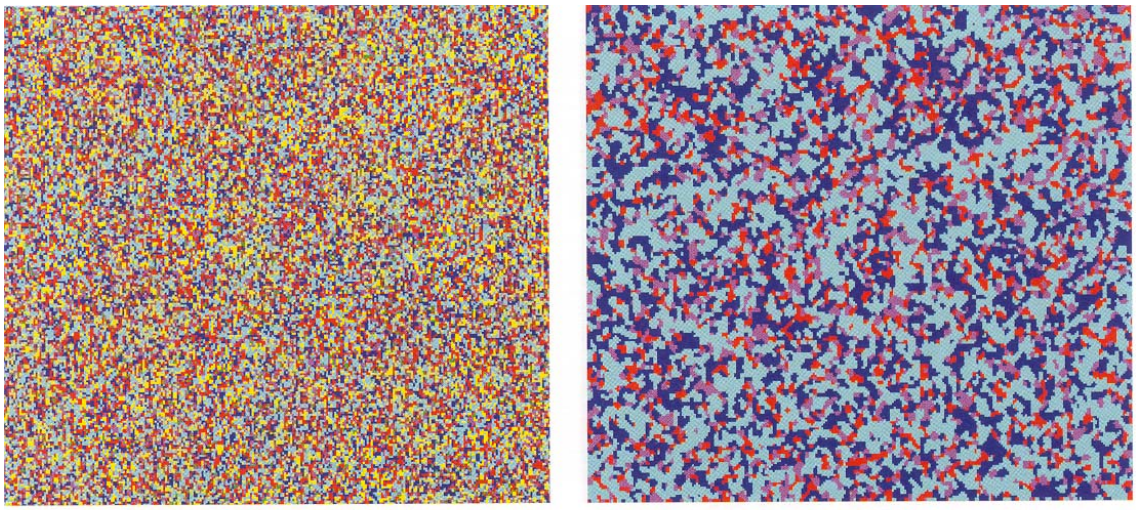

Figura 9. Worst ML (1) and ICM (r) classifications obtained, respectively, using C band, HH-HV phase difference information

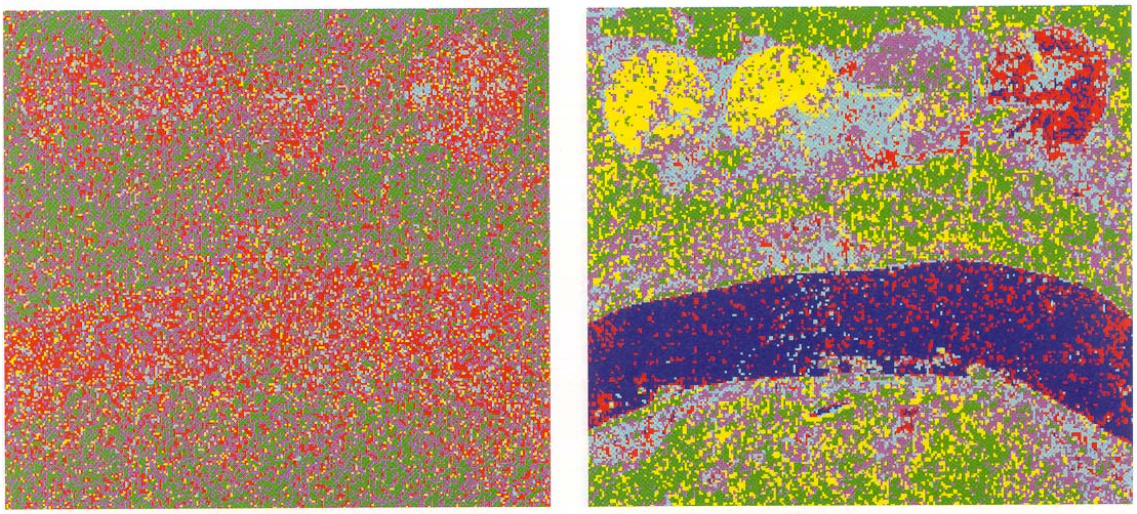

Figura 10. Worst (1) and best (r) ML classifications obtained, respectively, using L band, HH-HV ratio of intensities data and HV-VV intensity pair information

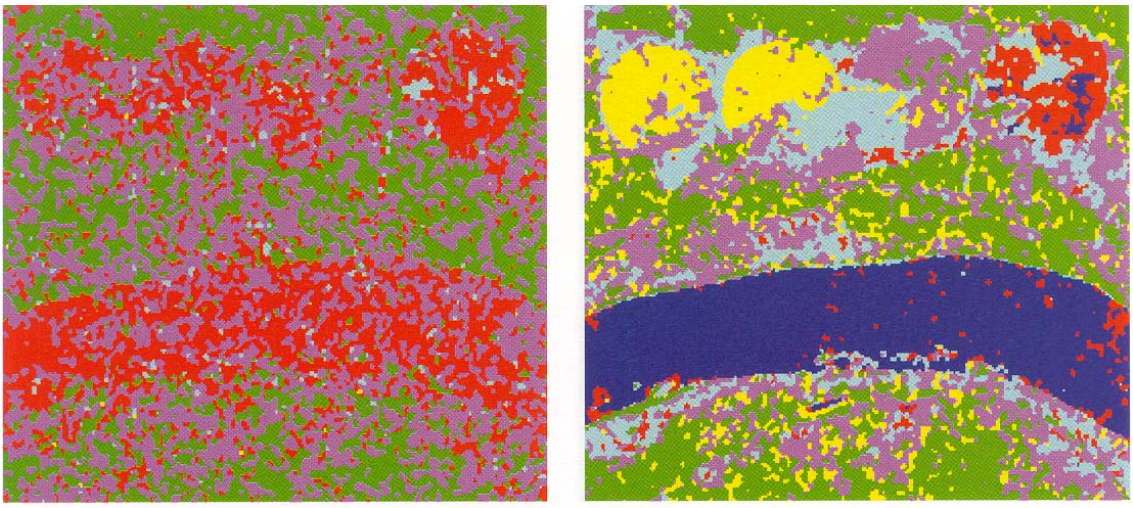

Figura 11. Worst (1) and best (r) ICM classifications obtained, respectively, using band, C, HH-HV phase difference data and band L, HV-VV intensity pair information

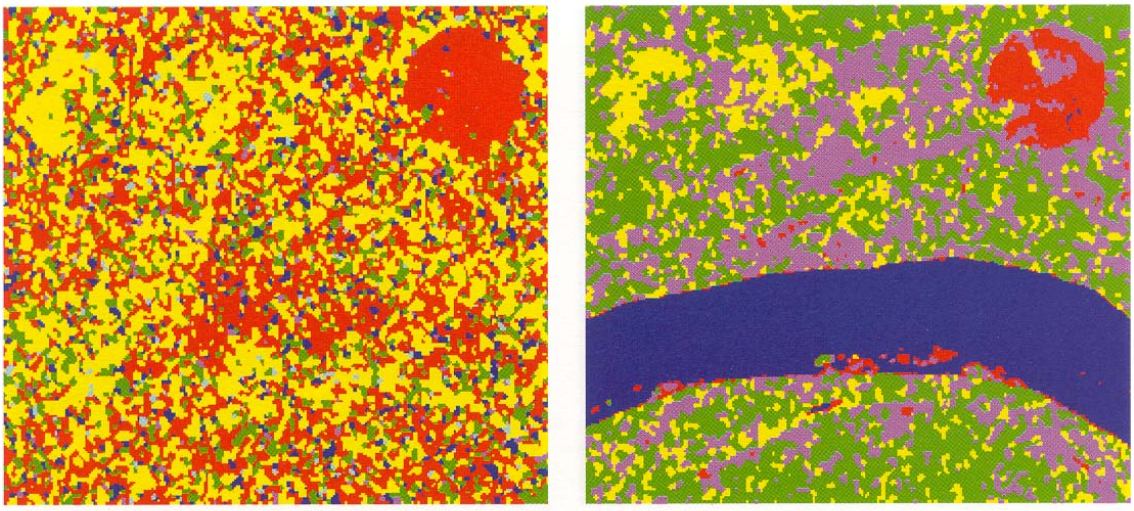

Figura 12. Worst (1) and best (r) ICM classifications obtained, respectively, using C band, HH-HV phase difference data and HH-HV intensity pair information